Electronic Supplementary Material (ESI) for Journal of Materials Chemistry A.

Supporting Information

An all-solid-state-supercapacitor possessing a non-aqueous gel polymer electrolyte prepared using a UV-assisted *in-situ* polymerization strategy

Vidyanand Vijayakumar[a,d], Bihag Anothumakkool[a,c,‡], Arun Torris A.T[b,‡], Sanoop B. Nair[b], Manohar V. Badiger[b,d]* and Sreekumar Kurungot[a,d]*

[a.] Physical and Materials Chemistry Division, CSIR-National Chemical Laboratory, Pune, Maharashtra, India – 411008. E-mail: k.sreekumar@ncl.res.in
[b.] Polymer Science and Engineering Division, CSIR-National Chemical Laboratory, Pune, Maharashtra, India – 411008. E-mail: mv.badiger@ncl.res.in
[c.] Electrochemical Storage and Conversion of Energy Institut de Matériaux de Nantes, France
[d.] Academy of Scientific and Innovative Research (AcSIR), CSIR-NCL Campus, Pune, Maharashtra, India – 411008

CONTENTS

S/No.	Title of the Section	Page No.
1.	Details of Electrochemical Characterisations.	3
2.	Device Fabrication.	3
3.	NMR spectrum of the HPA monomer and PHPA. (Fig. S1(a) and (b))	4
4.	Mechanical properties of PHPA, H-P-80%, GPEs and electrodes. (Fig. S2)	5
5.	ATR-FTIR spectral investigation. (Fig. S3)	6
6.	Structure of the Monomers used. (Fig. S4)	7
7.	Nyquist plot of the M-P-L-3M-60% GPE. (Fig. S5)	8
8.	FE-SEM image, EDX analysis and BET adsorption-desorption isotherms of YP-80F. (Fig. S6)	9
9.	Dimension of the HPA monomer. (Fig. S7)	9
10.	Electrochemical characterisation of the supercapacitor devices. (Fig. S8,S9,S10 and S11)	10-11
11.	Comparison between the in-situ and conventional device fabrication strategies. (Fig. S12 and S13)	12
12.	EDX mapping of the carbon sample after the in-situ polymerization. (Fig. S14)	13
13.	Cross sectional FE-SEM image of the H-P-L-3M-S-3.8 and PMMA-PC-L-3M-S-3.8 device. (Fig. S15)	13
14.	Comparison of mechanical stability of Bare electrode and GPE coated electrode. (Fig. S16 and S17)	14
15.	Specific capacitance of the scaled up devices at various current densities in the scale of A g^{-1}. (Fig. S18)	15
16.	Comparison and summary of the current work to already reported works in the literature. (Table. 1)	16

1. Electrochemical Characterizations[1]

The equation (1) is used for the calculation of Gravimetric capacitance (F g^{-1}) from the charge-discharge method.

$$C = \frac{2 \times (I \times \Delta t)}{\Delta V * M} \quad (1)$$

where,

Δt = Discharge time
ΔV = Potential window
I = Constant current used for charging and discharging
M = Weight of active carbon material in one of the electrode

The obtained device capacitance was multiplied by a factor of 2 in order to get the single electrode capacitance which is included in **Equation 1**.
Gravimetric energy density (E_d) and power density (P_d) were calculated from the capacitance value obtained from the charge-discharge method.

Energy density (E_d) (Wh kg^{-1}) $= \frac{Cs}{8 \times 3.6} V^2$ (2)
where,
'Cs' is the specific capacitance calculated by the charge-discharge (F g^{-1}) method and 'V' is the voltage window.

Power density (P_d) (W kg^{-1}) $= \frac{Ed}{t}$ (3)

where, 'E_d' is the energy density from **Equation 3** and 't' is the discharge time in hour calculated from the discharge curve.

The ionic Conductivity of the GPEs films were calculated from the equation (5).

$$\rho\ (\Omega\ cm) = \frac{RA}{l} \quad (4) \qquad \sigma\ (S\ cm^{-1}) = \frac{1}{\rho} \quad (5)$$

σ= Conductivity of the membrane
ρ = Resistivity of the membrane
R = bulk resistance of the membrane
A = Area of the membrane
l = Thickness of the membrane

2. Device fabrication

Fabrication of the *ex-situ* and M-P-L-3M-60%-S-3.0 devices

The supercapacitor device was fabricated using an *ex-situ* strategy where the H-P-L-3M-80% GPE film (Thickness = 0.25 mm) was prepared first in a Teflon mould and then sandwiched in between two electrodes as in the case of device fabrication using the conventional dry polymer electrolytes. The hence prepared device is hereafter termed as H-P-L-3M-S-*ex-xitu*, where 'S' stands for the solid device. The electrode mass loading was 3.0 mg cm^{-2}.
The supercapacitor device fabricated using the *in-situ* prepared M-P-L-3M-60% GPE is hereafter termed as M-P-L-3M-60%-S-3.0, where 'S' stands for the solid device and '3.0' stands for the electrode mass loading. The procedure used for the device fabrication is the same as it was used for the preparation of the HPA based devices except the fact that the pre-polymerised solution used in the case of MMA based device is M-P-L-3M-60%.
The electrochemical performance of the M-P-L-3M-60%-S-3.0 and the H-P-L-3M-S-*ex-xitu* devices were compared with the HPA based solid-state and liquid-state devices.

3. NMR spectrum of the HPA monomer and PHPA.

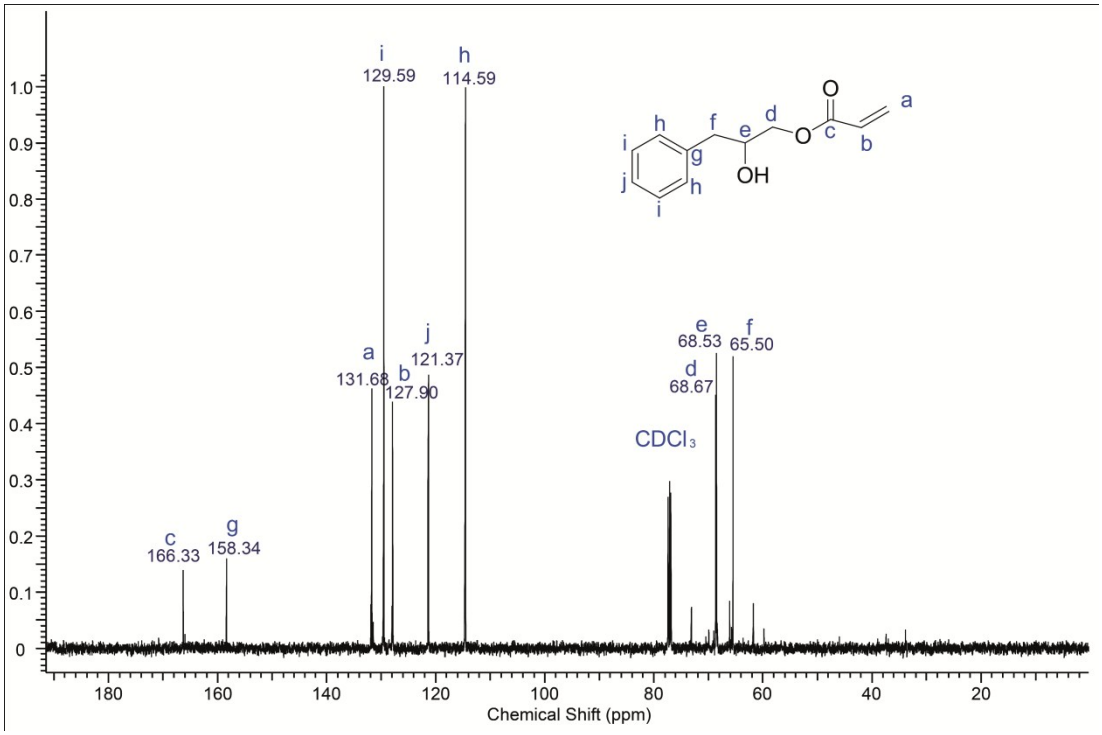

Fig. S1a ^{13}C-NMR spectra of the HPA monomer.

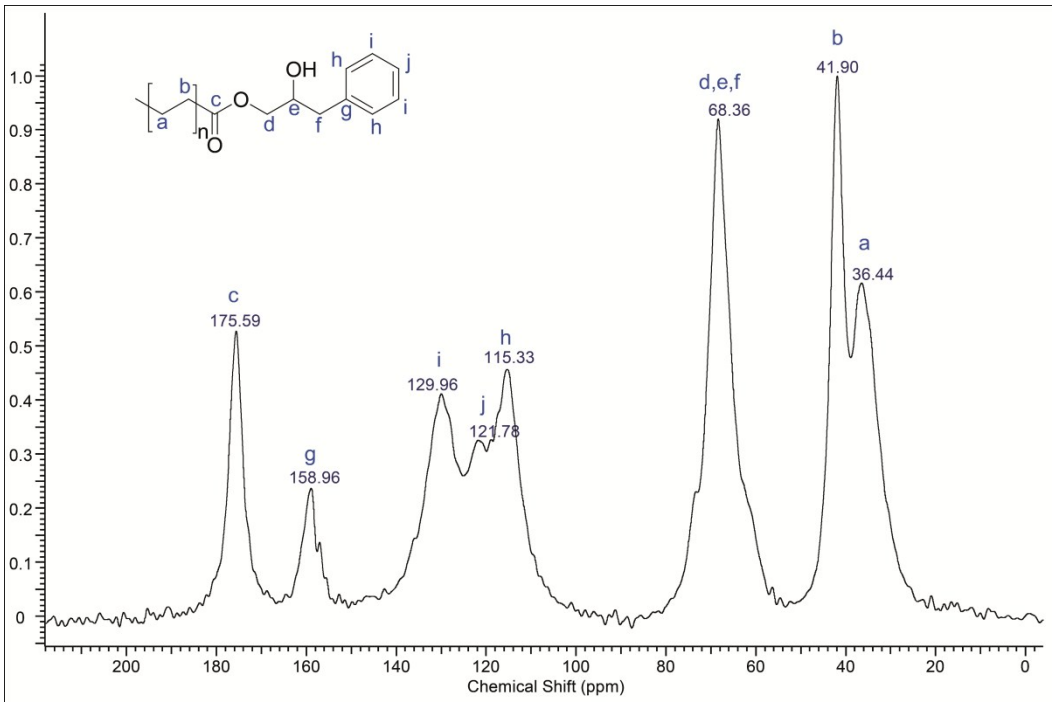

Fig. S1b ^{13}C-NMR spectra of PHPA polymer.

4. Mechanical properties of PHPA, H-P-80%, GPEs and electrodes

1. Dynamic mechanical analysis.

Dynamic mechanical analyzer (DMA) (RSA III, TA Instruments USA) equipped with TA Orchestrator software (Version 7.2.0.4) was used for the uni-axial tensile measurements (static mode) and dynamic compression measurements (dynamic mode) of H-P-L-xM-y% GPEs. For the uni-axial tensile measurements, H-P-L-3M-80% GPE specimens with a rectangular geometry of 5 mm width, 0.8 mm thickness and 15 mm length were prepared. Specimens were clamped onto tensile grips with a constant torque of 20 cN.m and applied the load at a speed of 1 mm min^{-1} up to failure. Dynamic mechanical measurements were performed on cylindrical specimens (8 mm dia. x 8 mm height) of neat PHPA, H-P-80% and H-P-L-xM-80% (x = 1,2 and 3) GPEs. Initially, linear visco-elastic region (LVR) of the gels was identified by performing linear strain sweep measurements followed by frequency sweep analysis to measure the modulus of the specimens in the range 0.1 to 10 Hz at ambient temperature.

For the uni-axial tensile measurements of the electrodes, two sets of electrodes were prepared. One set of electrodes coated with carbon and another set with carbon as well as photo-polymerized gel electrolyte. Electrode dimensions were 20 mm width, 0.5 mm thickness and 40 mm height. Electrodes were loaded onto the tensile grips of universal testing machine (Model: Instron 5943, Instron Ltd., MA, USA) with the aid of elastomeric strips on both side of the electrodes to avoid slippage during measurements. A pre-load to 0.01 N is applied to rectify the alignment and tensile test is performed upto rupture at the cross-head speed of 3 mm/min.

2 . Uni-axial un-confined compression and cyclic compression measurements

Uni-axial un-confined compression and cyclic compression measurements were performed with cylindrical H-P-L-3M-80% and H-P-80% gels of 15 mm diameter and 15 mm height using single column table top electro-mechanical material testing station of 1kN load cell capacity (Model: Instron 5943, Instron Ltd., MA, USA), equipped with cylindrical compression platens of 50mm diameter and Bluehill 3 software with TestProfiler module for recording as well as analysis of data sets. To prevent slippage and displacement of gels during the measurements, both compression plate surfaces were glued with sand-coated paper of grade 100 (Multicut Paper, Vinal Abrasives, India). A pre-load of 0.01 N is applied prior to compression measurements to attain uniform contact between the surface of gels and compression platens. A cross-head speed of 10 mm min^{-1} is used for all compression measurements with ±0.1% speed and position accuracy. Minimum of 3 samples were measured and representative histograms were plotted.

Uni-axial compression was performed on H-P-L-3M-80% and H-P-80% gels up to 98% compression or till specimen failure, whichever is earlier. Two sets of the uni-axial cyclic compression measurements were performed on cylindrical H-P-L-3M-80% and H-P-80% gels with the first set of measurement comprising of a sequence of 8 or 9 cyclic measurements with varying compressive strain starting from 10 to 80 or 90 %. The second set of cyclic measurement involves continuous 200 cycles of compression at constant 70 or 90% compressive strain without interval. The samples used were having a dimension of Hysteresis energy is calculated from the histogram of compressive stress versus compressive strain following **Equation 6**[2] given below:

$$U_{90\%} = \frac{\int_{0}^{0.9_{loading}} F \mathrm{d}s - \int_{0}^{0.9_{unloading}} F\, \mathrm{d}s}{\pi r^2} \quad \ldots\ldots\ldots\ldots\ldots\ldots\ldots\ldots (6)$$

where, '$U_{90\%}$' represents the dissipated energy for 90% compressive strain, 'F' is the loading, 's' is the displacement to the corresponding strain and 'r' is the radius of the gel.

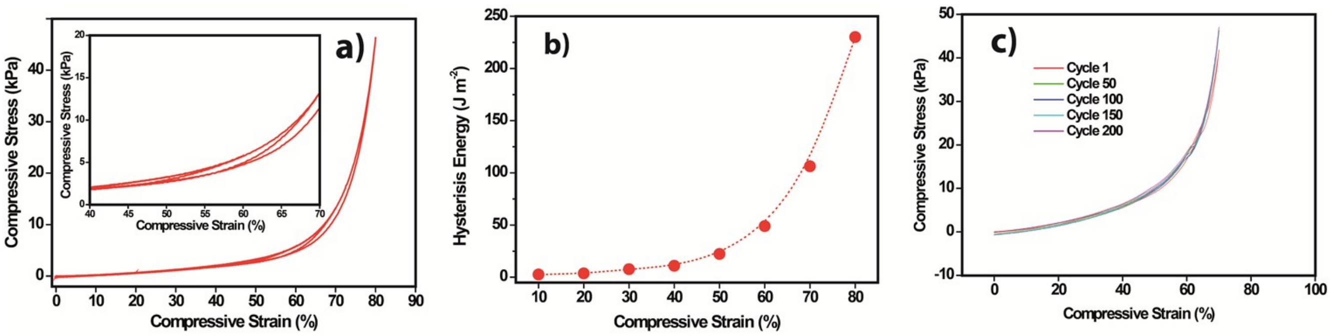

Fig. S2 (a) Sequential uni-axial compression cycles of H-P-80% from 10 to 80% strain where the inset shows the maximum stress per cycle versus the corresponding strain from 40% to 70% compression strain; (b) hysteresis energy of the sequential uni-axial compression cycles from 10 to 80% compressive strain for H-P-80%; (c) Compressive stress vs. Compressive strain plot recorded for 200 repeated cycles of uni-axial compression for H-P-80% gel at an interval of each 50 cycles.

5. ATR-FTIR spectral investigation

From **Figure 2c**, comparing the FTIR spectrum of the monomer and neat PHPA, the peak corresponding to the C=C stretching at 1629 cm^{-1} is present in the monomer, whereas, it is absent in the case of the polymer PHPA. The C=O stretching band of the monomer is observed at 1717 cm^{-1}, whereas, in the polymer, it is shifted to a frequency of 1729 cm^{-1}. This is due to the difference between the α,β-unsaturated conjugated carbonyl in acrylate double bonds and the α,β-saturated conjugated carbonyl in the polymer.[3] This further confirms that the polymerisation is complete which is already been proved from NMR. In the spectrum of H-P-80%, the peak corresponding to the carbonyl group of the polymer matrix of PHPA shows a shift from 1729 cm^{-1} to 1737 cm^{-1}. This blue shift can be attributed to the hindrance to the hydrogen bonding present in the polymer matrix, once the plasticizer solvent (PC) is introduced into the system. In the case of pure PC, the FTIR data shows a peak at 1781 cm^{-1} which corresponding to the stretching mode of the C=O group of PC.[4] In the GPEs, this peak (1781 cm^{-1}) shows a gradual redshift as the concentration of the $LiClO_4$ is increased. This is attributed to the interaction between the carbonyl group of PC and the Li^+ cation. At the same time, it is observed that the peak at 1737 cm^{-1} also shows a shift towards lower frequency when the $LiClO_4$ is introduced and on successive increment in the concentration of $LiClO_4$, the peak is disappeared. The disappearance of the peak is due to the broadening of the peak corresponding to the carbonyl group of PC, where, it is merged with the carbonyl peak of the polymer matrix. Moreover the amount of the solvent is excess in the system compared to the polymer, which also contributes to the disappearance of the carbonyl band of the polymer matrix. The increase in the intensity of the peak at 624 cm^{-1} as the concentration of $LiClO_4$ increases in the gel polymer electrolyte is attributed to the increase in amount of the free ClO_4^- ions. This confirms the improved dissociation of the conducting salt in the H-P-L-3M-80% gel polymer electrolyte compared to the others.

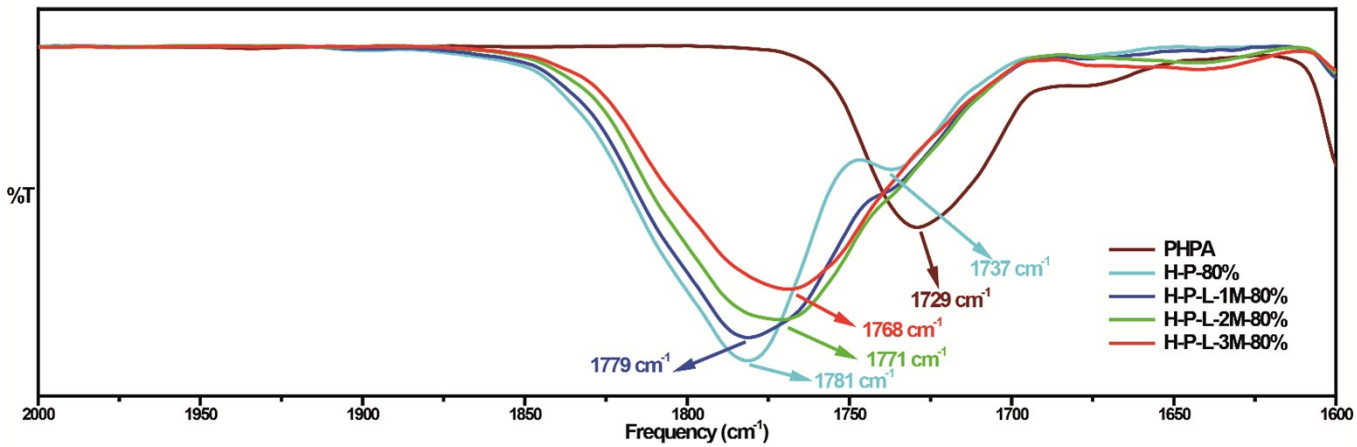

Fig. S3 ATR-FTIR spectra magnified between 1600 cm^{-1} to 2000 cm^{-1}.

6. Structure of the Monomers used

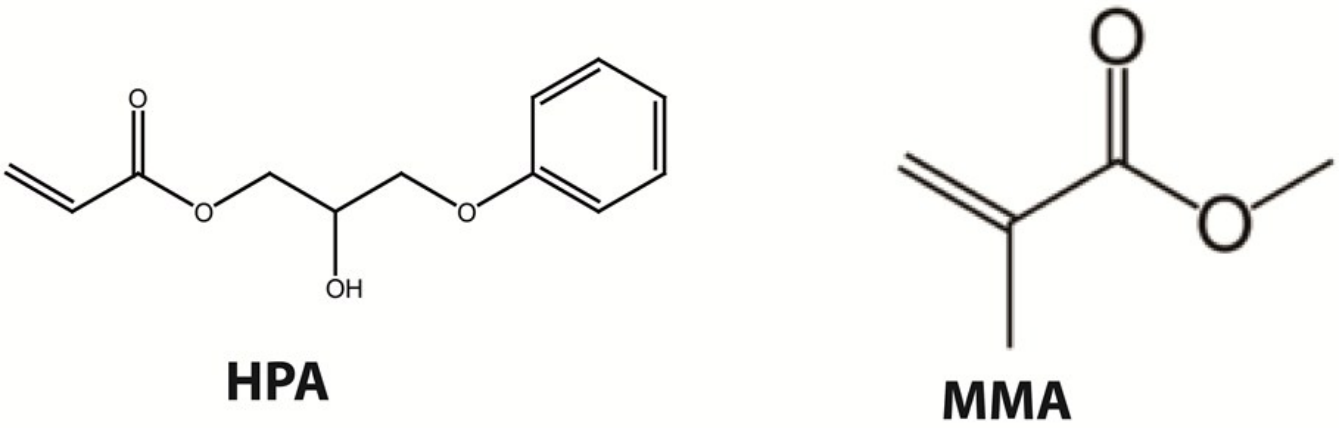

Fig. S4 The structure of the HPA and MMA monomers.

7. Nyquist plot of the M-P-L-3M-60% GPE

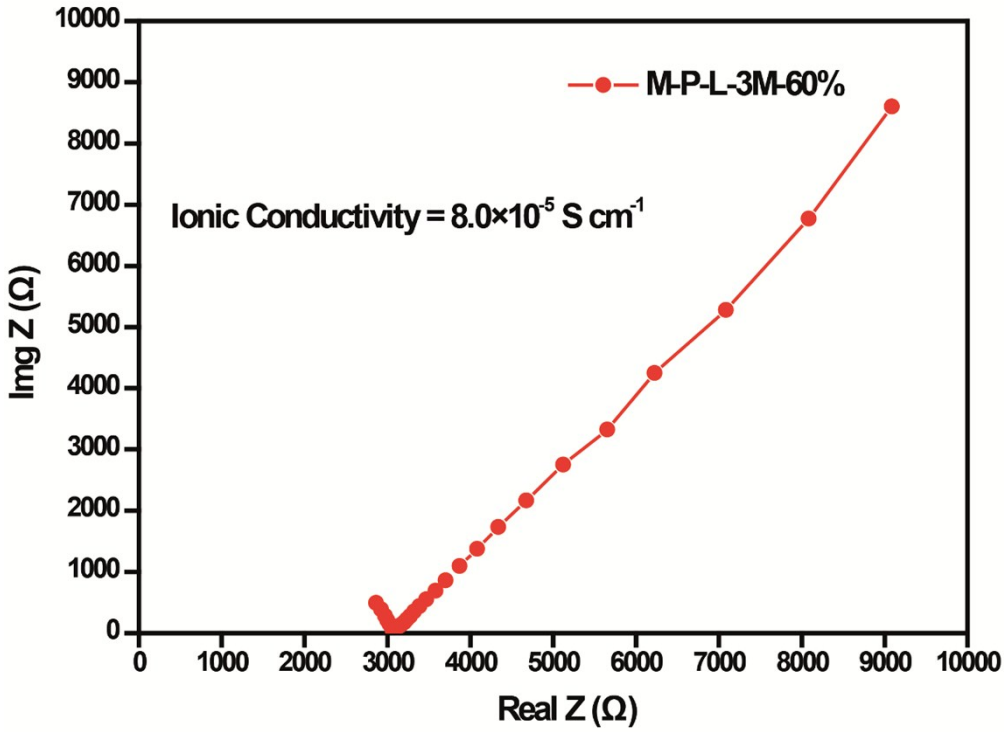

Fig. S5 Nyquist plot of the M-P-L-3M-60% GPE.

8. FE-SEM image, EDX analysis and BET adsorption-desorption isotherms of YP-80F.

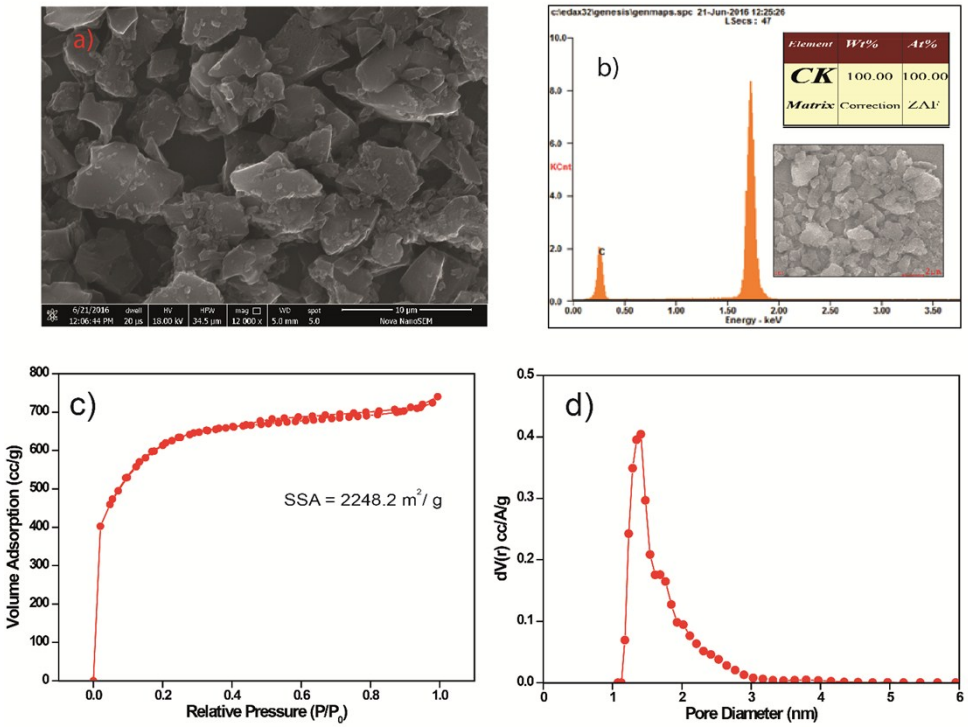

Fig. S6 (a) FESEM image of YP-80F; (b) EDAX of YP-80F; (c) N_2-adosption isotherm of the carbon (YP-80F) used for preparing the electrode for the supercapacitor; (d) Pore-size-distribution profile of the carbon powder used for making the device.

9. Dimension of the HPA monomer

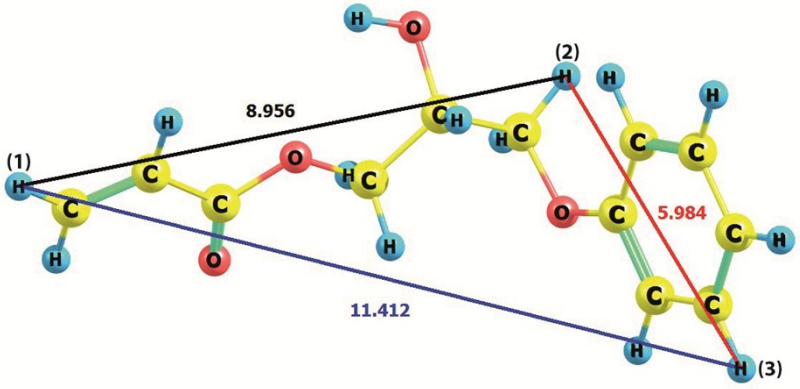

Fig. S7 Optimized conformation of the monomer (HPA) at PBE/TZVP level of theory. Distances between the hydrogen atoms are given in Angstrom (Å) unit.

Full quantum mechanical calculations were done with density functional theory (DFT) at the PBE/TZVP[5, 6] level of theory using Turbomole 7.0 program[7] in order to gain further insight into the dimension and geometry of the HPA monomer. The optimized geometry is shown in **Figure S7**. The maximum distance between the two terminal atoms (H(1) and H(3)) is 11.412 Å, which is very much less than that of the carbon pore size (10-15 Å). The XYZ coordinates of the PBE/TZVP optimized geometry are given at the end of SI (**Page No.17**).

10. Electrochemical characterisation of the supercapacitor devices

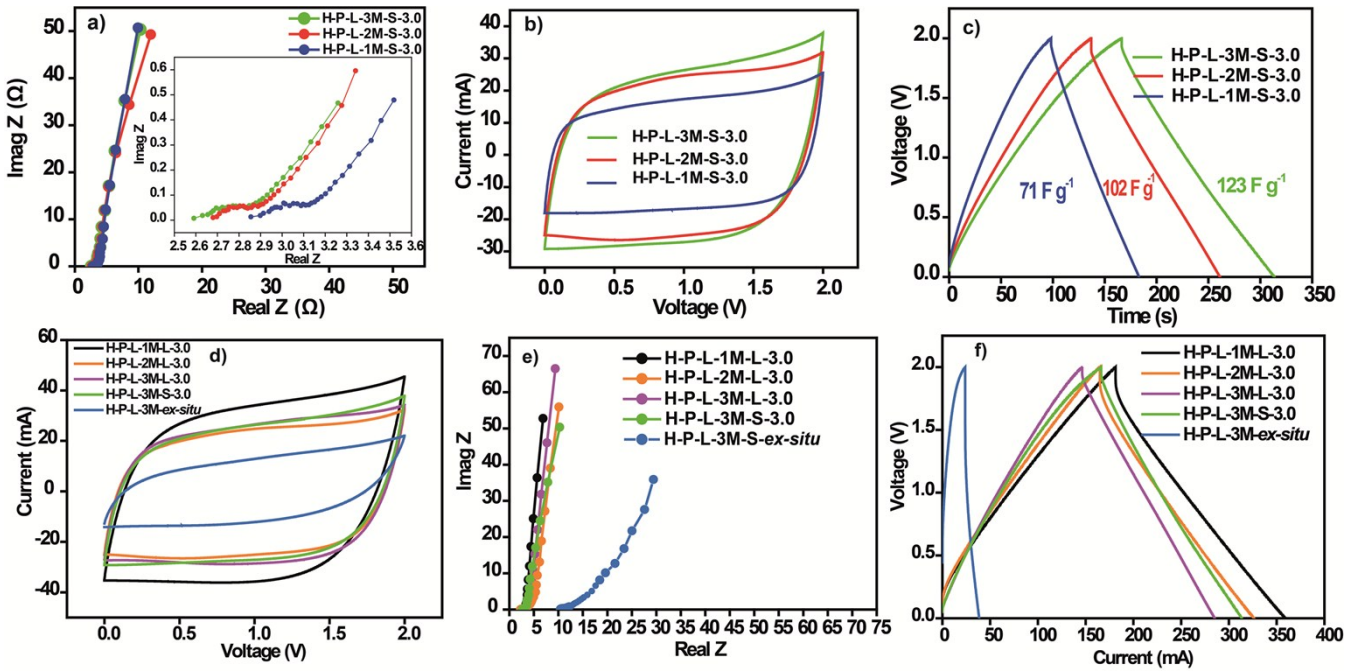

Fig. S8 (a) to (c) Combined Nyquist plot (a), CV profile recorded at a scan rate of 50 mV s^{-1} (b) and CD profile recorded at a current density of 2 mA cm^{-1} (c) for the supercapacitor devices: H-P-L-xM-S-3.0, where 'x'= 1,2 and 3; (d) to (f) The combined CV profile at a scan rate of 50 mV s^{-1} (d), Nyquist plot (e) and the CD profile recorded at a current density of 2 mA cm^{-2} (f) taken for the various liquid-state and solid-state devices under the study.

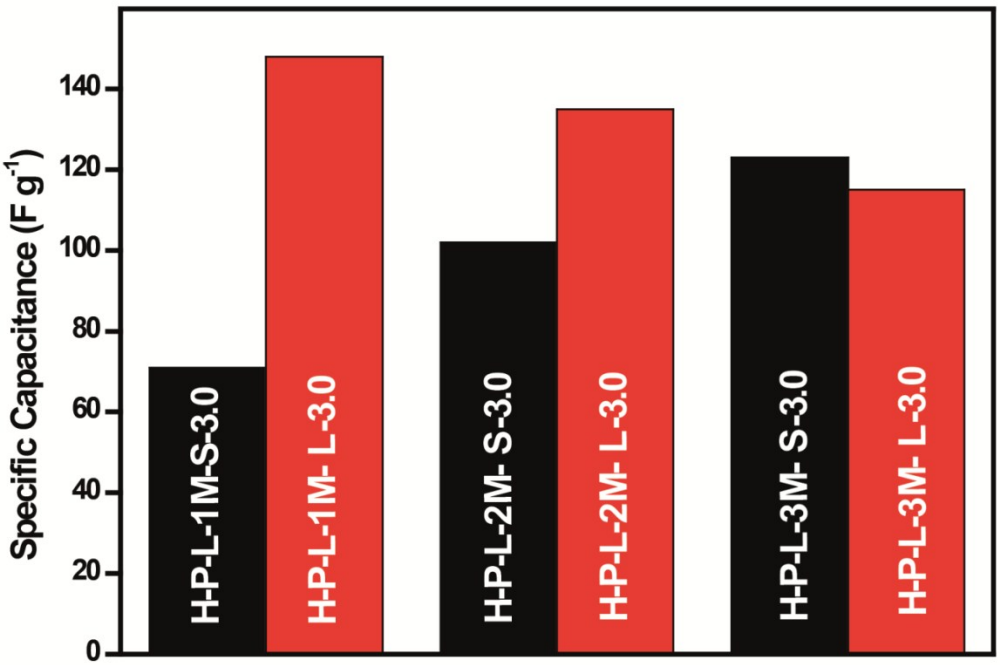

Fig. S9 Comparison of the Specific capacitance values obtained for the various devices at a current density of 2 mA cm^{-1}.

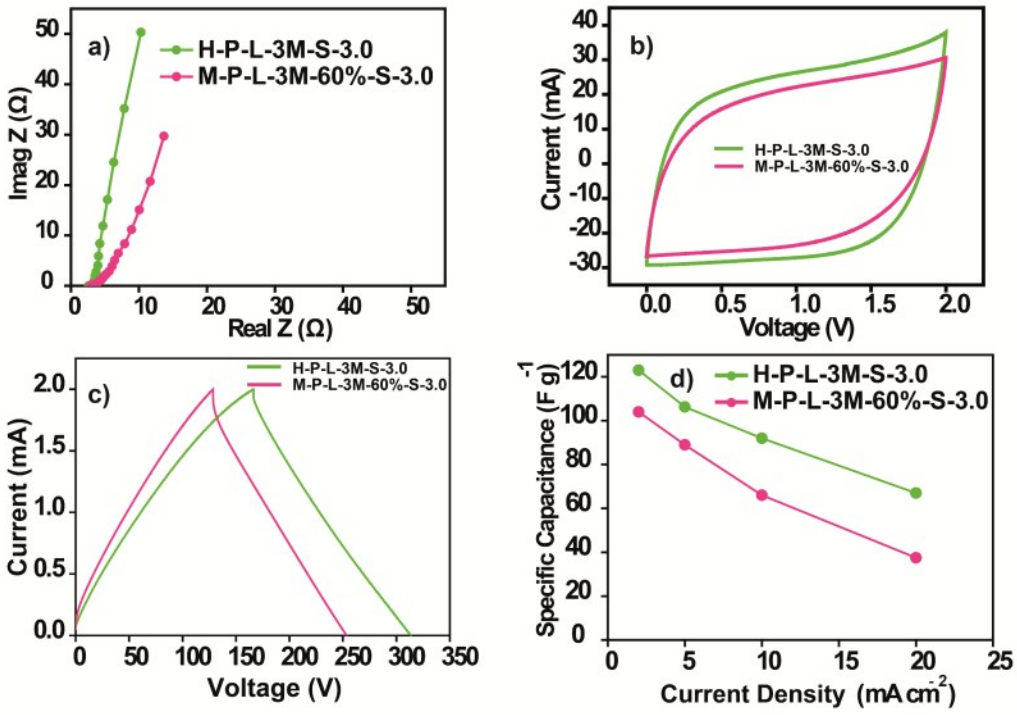

Fig. S10 (a) to (c) Combined Nyquist plot (a), CV profile recorded at a scan rate of 50 mV s^{-1} (b) and CD profile recorded at a current density of 2 mA cm^{-1} (c) for the supercapacitor devices: H-P-L-3M-S-3.0 and M-P-L-3M-60%-S-3.0 ; (d) plots representing the Mass Specific Capacitance *vs.* Current Density for the H-P-L-3M-S-3.0 and M-P-L-3M-60%-S-3.0 devices.

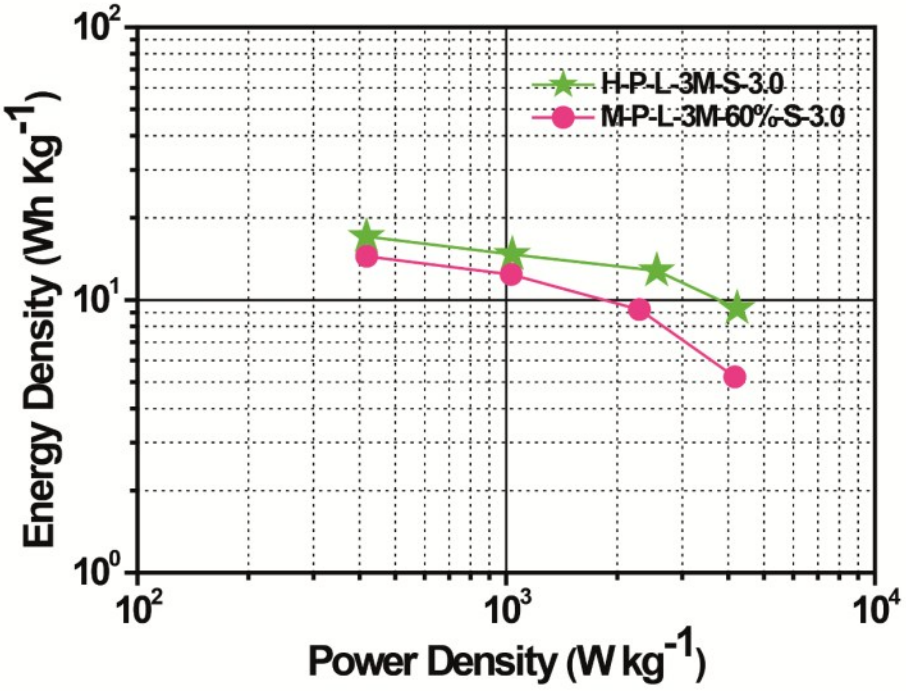

Fig. S11 Combined Ragone plot comparing the energy and power density of H-P-L-3M-S-3.0 and M-P-L-3M-60%-S-3.0 supercapacitor devices.

11. Comparison between the *in-situ* and conventional device fabrication strategies

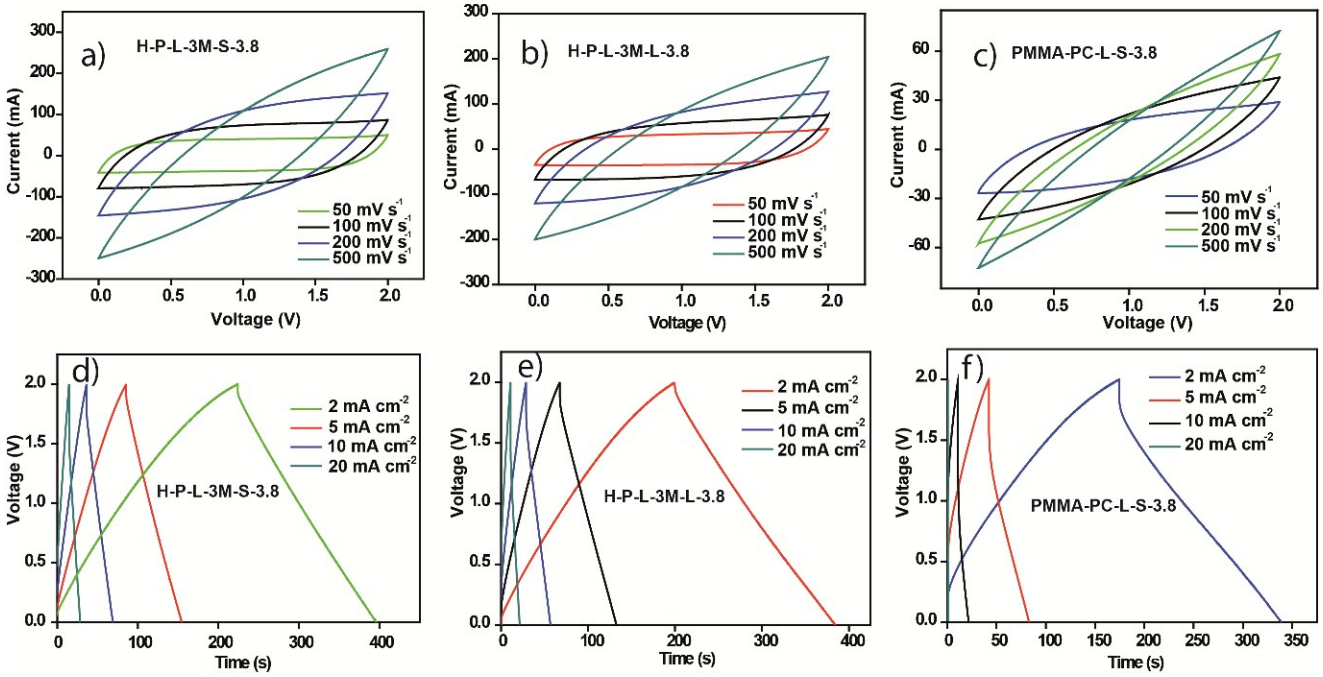

Fig. S12 (a) to (c) Complete CV profiles of the supercapacitor devices: H-P-L3M-S-3.8 (a), H-P-L-3M-L-3.8 (b) and PMMA-PC-L-S-3.8 (c) ; (d) to (f) complete CD profiles of the H-P-L-3M-S-3.8 supercapacitor devices: H-P-L-3M-S-3.8 (d), H-P-L-3M-L-3.8 (e) and PMMA-PC-L-S-3.8 (f).

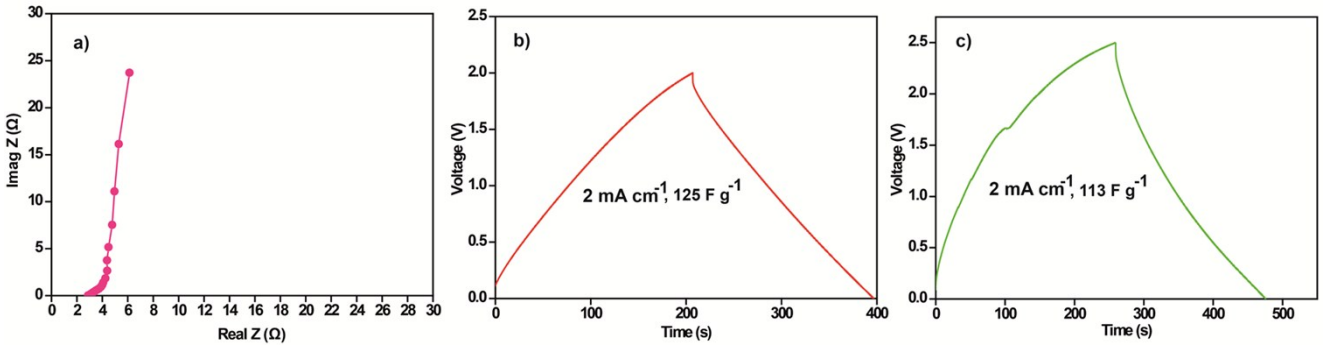

Fig. S13 Charge-discharge profile recorded for the YP-80F carbon at a current density of 2 mA cm^{-2} in standard non-aqueous electrolyte (3 M $LiClO_4$/PC) at (a) 2.0 V window (b) 2.5 V window.

12. EDX mapping of the carbon sample after the *in-situ* polymerization

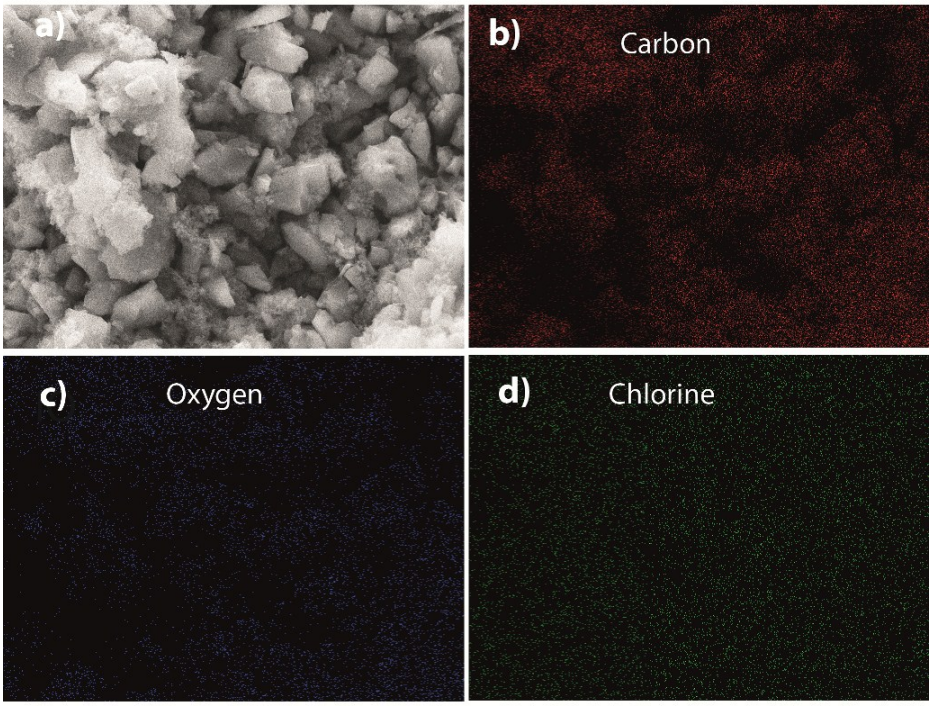

Fig. S14 EDX mapping of the carbon sample after the *in-situ* polymerization: (a) carbon portion which is taken after the *in-situ* polymerization from the device; (b)-(d) elemental mapping of carbon (b), Oxygen (c) and Chlorine (d) which are corresponding to the area represented in (a).

13. Cross sectional FE-SEM image of the H-P-L-3M-S-3.8 and PMMA-PC-L-3M-S-3.8 device

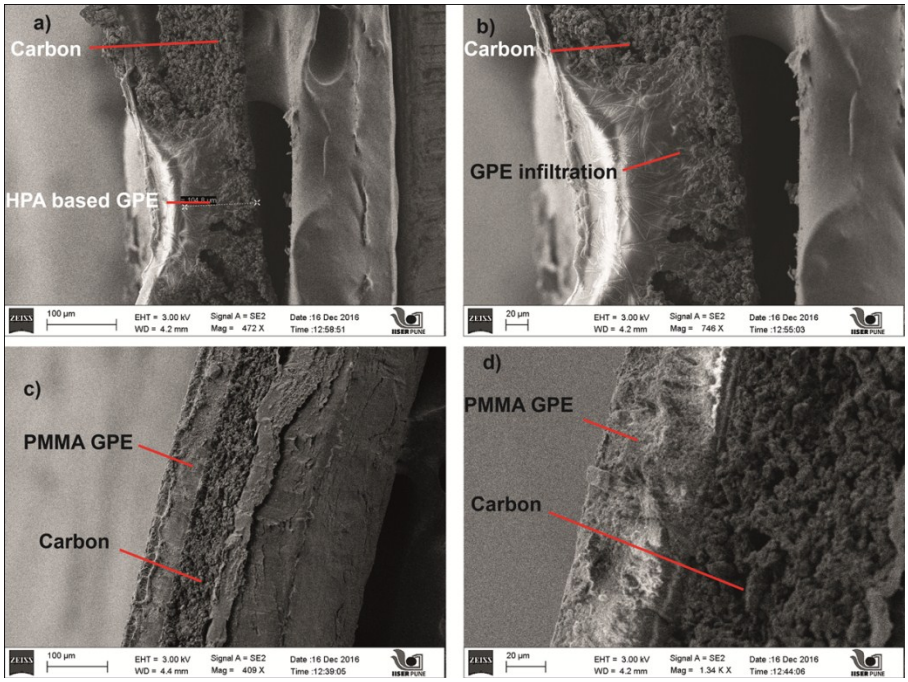

Fig. S15 (a) and (b) The cross sectional FE-SEM image of the H-P-L-3M-S-3.8 device; (c) and (d) The cross sectional FE-SEM image of the PMMA-PC-L-3M-S-3.8 device.

14. Comparison of mechanical stability of Bare electrode and GPE coated electrode.

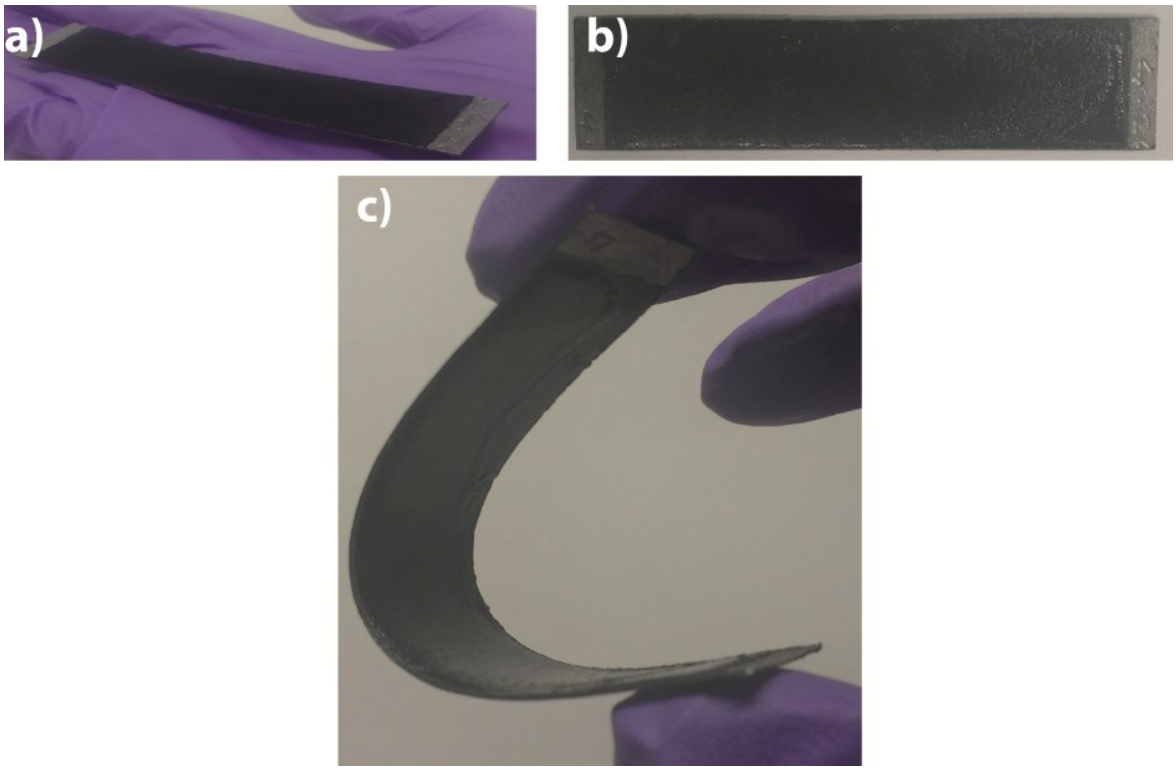

Fig. S16 (a) Blank-electrode before the *in-situ* GPE generation; (b) Electrode after the *in-situ* GPE generation; (c) The electrode in bent condition after the *in-situ* GPE generation.

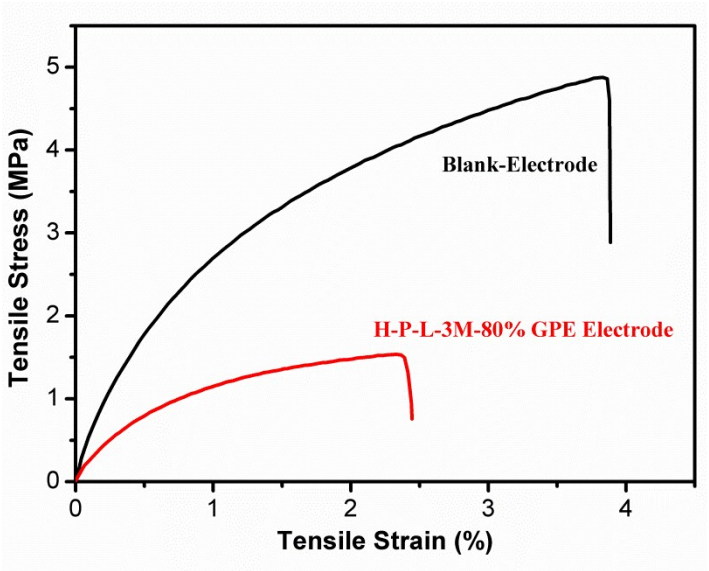

Fig. S17 Tensile stress *vs.* tensile strain plot of electrodes with and without GPE.

15. Specific capacitance of the scaled up devices at various current densities in the scale of A g^{-1}.

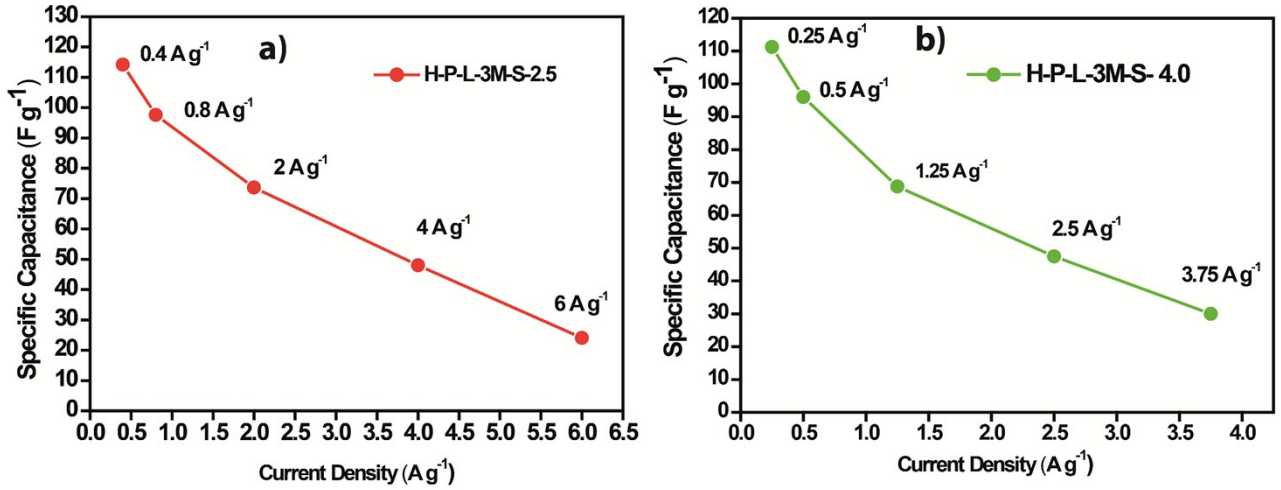

Fig. S18 The specific capacitance of the devices H-P-L-3M-S-2.5 (a) and H-P-L-3M-S-4.0 (b) at various current densities in the scale of A g^{-1}.

16. Comparison and summary of the current work to already reported works in the literature

Active Electrode material	GPE used	Details of Device Fabrication	ESR	Specific Capacitance	Reference
1. YP-80F	Poly (HEMA-co-MMA) with DPHPO4	GPE film is used, Tested the device in Sweaglock Cell, Electrodes pre-soaked with Electrolyte, Electrode area = 1.28 cm^2, Active material loading = 2 mg cm^{-2}.	95 Ω cm^2	123 F g^{-1} at 0.78 mA g^{-1}	11 Main Text
2. CNT	Silica Nano-Powder with [EMIM][NTf_2]	Quasi-solid state Gel electrolyte pressed in between the electrodes, Electrode area = 1 cm^2, Low Active material loading = 0.23 mg cm^{-2}.	30 Ω	135 F g^{-1} at 2 A g^{-1}	68 Main Text
3. AC	Poly (OEGMA-co-BnMA)	Organic electrolyte swollen GPE film is used, Area of the device = 1.13 cm^2, Mass loading = Mass loading=3.1 mg cm^{-2}.	20 Ω cm	24 F g^{-1} at at 0.8 A g^{-1}	23 Main Text
4. AC	PEO-NaTFSI	Quasi-solid state GPE, Electrode area= 1 cm^2, Active material loading 4-5 mg, Device testing details are not provided.	6.8 Ω	25.6 F g^{-1} at 200 mA g^{-1}	69 Main Text
5. CNT	PS-PEO-PS tri-block copolymer with [EMIM][NTf2]	Quasi-solid-state GPE spread over electrode, Device area = 1 cm^2, Loading not mentioned.	31.3 Ω	50.5 F g^{-1} at at 1 A g^{-1}	21 Main Text
6. YP-80F	H-P-L-3M-80%	*In-situ* GPE generation, Solid-state GPE, Electrode Area = 16 cm^2, Mass loading= 4.5 mg cm^{-2}	2.2 Ω	111 F g^{-1} at 0.20 A g^{-1}	This Work

Table 1 : The electrochemical performances among the GPE based supercapacitor devices already reported in the literatures and the devices reported in this work are compared and summarised.

References

1. W. Chen, Z. Fan, L. Gu, X. Bao and C. Wang, *Chemical Communications*, 2010, **46**, 3905-3907.
2. J. Wei, J. Wang, S. Su, S. Wang and J. Qiu, *Journal of Materials Chemistry B*, 2015, **3**, 5284-5290.
3. T. Y. Lee, T. M. Roper, E. S. Jönsson, C. A. Guymon and C. E. Hoyle, *Macromolecules*, 2004, **37**, 3659-3665.
4. S. Sopeña, G. Fiorani, C. Martín and A. W. Kleij, *ChemSusChem*, 2015, **8**, 3248-3254.
5. J. P. Perdew, K. Burke and M. Ernzerhof, *Physical Review Letters*, 1996, **77**, 3865-3868.
6 A. Schäfer, C. Huber and R. Ahlrichs, *The Journal of Chemical Physics*, 1994, **100**, 5829-5835.

7. TURBOMOLE V7.0 2015, a development of University of Karlsruhe and Forschungszentrum Karlsruhe GmbH, 1989-2007, TURBOMOLE GmbH, since 2007; available from http://www.turbomole.com.

The XYZ coordinates of the PBE/TZVP optimized geometry.

30

C	0.183106	1.223204	0.163768
C	0.398570	1.001557	1.465267
H	-0.235558	2.174431	-0.172097
H	0.417605	0.469738	-0.588972
H	0.817281	0.062629	1.832642
C	0.074176	2.035022	2.479496
O	-0.377788	3.144080	2.263795
O	0.357769	1.566418	3.735904
C	0.071032	2.481780	4.826432
H	0.731022	3.359454	4.761476
H	-0.975942	2.815435	4.755032
C	0.309426	1.703417	6.108840
H	1.365028	1.369565	6.126568
O	-0.575302	0.585130	6.222521
H	-0.508845	0.091643	5.385383
C	0.037482	2.578210	7.336694
H	-0.938741	3.073385	7.235317
H	0.001166	1.941955	8.235150
O	0.989693	3.636084	7.468013
C	2.212559	3.363546	8.038752
C	3.091518	4.455698	8.112998
C	2.607045	2.114835	8.540855
C	4.349393	4.299561	8.688788
C	3.873812	1.976383	9.120598
C	4.750364	3.058582	9.199537
H	2.762421	5.417483	7.716730
H	1.947899	1.248418	8.487304
H	5.023272	5.157041	8.740770
H	4.171489	1.001222	9.511266
H	5.736224	2.939905	9.651244